metals

MDPI

Article

Kinetic Analysis of the Transformation from 14M Martensite to $L2_1$ Austenite in Ni-Fe-Ga Melt Spun Ribbons

Alejandro F. Manchón-Gordón [1], Raúl López-Martín [1,2], Jhon J. Ipus [1], Javier S. Blázquez [1,*], Peter Svec, Sr. [3], Clara F. Conde [1] and Alejandro Conde [1]

[1] Dpto. Física de la Materia Condensada, ICMSE-CSIC, Universidad de Sevilla, P.O. Box 1065, 41080 Sevilla, Spain; afmanchon@us.es (A.F.M.-G.); raul.lopez@uclm.es (R.L.-M.); jhonipus@us.es (J.J.I.); cfconde@us.es (C.F.C.); conde@us.es (A.C.)
[2] Instituto Regional de Investigación Científica Aplicada (IRICA), Dpto. Física Aplicada, Universidad de Castilla-La Mancha, Avda Camilo José Cela, 10, 13071 Ciudad Real, Spain
[3] Institute of Physics, Slovak Academy of Sciences, Dúbravská cesta 9, 845 11 Bratislava, Slovakia; peter.svec@savba.sk
* Correspondence: jsebas@us.es

Abstract: In this study, the non-isothermal kinetics of the martensitic transition from 14M modulated martensite to austenite phase in $Ni_{55}Fe_{19}Ga_{26}$ ribbons obtained by melt-spinning has been analyzed. The proximity of the martensitic transition to room temperature makes it very sensitive to pressure and subtle differences for different pieces of the ribbon (ascribed to stresses stored in the ribbon during its rapid solidification process). Despite the dispersion in the characteristic parameters of the transition, a general behavior is observed with a decreasing activation energy as the heating rate increases due to the nucleation driven character of the transition. It has been shown that a first-order autocatalysis can describe the temperature evolution of the austenite fraction using only two experimental temperatures. Predicted curves are in good agreement with experimental data.

Keywords: heusler; martensitic transformation; kinetic analysis; melt-spinning

Citation: Manchón-Gordón, A.F.; López-Martín, R.; Ipus, J.J.; Blázquez, J.S.; Svec, P., Sr.; Conde, C.F.; Conde, A. Kinetic Analysis of the Transformation from 14M Martensite to $L2_1$ Austenite in Ni-Fe-Ga Melt Spun Ribbons. *Metals* **2021**, *11*, 849. https://doi.org/10.3390/met11060849

Academic Editor: Carlos Garcia-Mateo

Received: 22 April 2021
Accepted: 18 May 2021
Published: 21 May 2021

1. Introduction

Since Ullako et al. [1] reported a large magnetic field induced strain in Ni_2MnGa single crystals, Heusler alloys have drawn much attention as potential candidates for many applications at room temperature. These are related to the martensitic transformation of these materials, which can be controlled via magnetic field or stress application [2–4]. Among these magnetic shape memory effect Heusler alloys, the most studied series are Ni-Mn-X (X = Ga, Sn, In) [5]. More recently, Fe substitution for Mn has been proposed to enhance ductility in these alloys in Ni-Fe-Ga alloys [6] and several studies have been devoted to these systems [7–9]. In order to produce them, rapid quenching techniques such as melt-spinning are effective single step production processes leading to textured polycrystalline ribbons without segregation of secondary phases. However, despite the homogeneous chemical composition achieved, this technique may give rise to a rich variety of micromodulated structures [10] resulting in a variety of martensite phases with similar energies and strongly affected by external stimuli (magnetic field [11], pressure [12], etc.).

The diffusionless martensitic transformation is a first-order phase transition from a high temperature, high symmetry austenite phase to a low temperature, low symmetry martensite phase. The kinetics of this transformation is characterized by a distribution of nucleation processes (described as avalanche phenomena [13]) and a collective motion of a relatively large number of atoms with a fast growth rate (in the order of the speed of sound [14]). These characteristics reduce the utility of the interpretation of the kinetics of martensitic transformations in the frame of classical nucleation and growth theory developed by Johnson and Mehl [15], Avrami [16,17] and Kolmogorov [18] (JMAK). In fact,

Avrami exponents equal to 1 [19] are indicative of lost information about the growth process (as it is predicted for instantaneous growth models used to described nanocrystallization processes [20]). In fact, the JMAK equation proposed for isothermal transformations:

$$X = 1 - exp\left(-[k(t - t_0)]^n\right), \quad (1)$$

where X is the transformed fraction, k the frequency factor, t the time and t_0 the induction time) can be recognized in the non-isothermal Koistinen–Marburger equation describing the martensite phase fraction in quenching processes [21]:

$$X = 1 - exp\left(-k'(M_S - T_q)\right), \quad (2)$$

In this equation, the temperature dependence of the kinetic parameters is neglected and, thus, $n = 1$ and $k' = k/\beta$ (where β the cooling rate), M_S is the martensitic start temperature and T_q the minimum achieved temperature during quenching.

On the other hand, martensitic transformation can be described as an first-order autocatalytic reaction for which the transformation rate is proportional to the amount of initial and final phases (assuming the simplest first order kinetic equation) [22]:

$$\frac{dX}{dt} = k_M X(1 - X), \quad (3)$$

where k_M is the corresponding frequency factor.

Particularly, in $Ni_{55}Fe_{19}Ga_{26}$ Heusler alloy, martensitic transformation is observed slightly above room temperature and thus, is very sensitive to external factors. The proximity of the Curie temperatures of the two phases to the structural transition temperature leads to magnetoelastic and magnetostructural changes. Therefore, pressure or magnetic field application do affect the transition characteristics. In fact, our previous results on melt-spun samples of this composition show the high sensitiveness of the transformation to mechanical treatments at room temperature, consisting of axial pressure application in the range of ~125 MPa [23]. After the load was removed, a permanent effect on the transition is observed, with a progressive reduction in the enthalpy of the transformation as the applied pressure increased from 25 to 125 MPa. This decrease in enthalpy was correlated with a progressive intermartensitic transition from the monoclinic modulated 14M phase to the non-modulated $L1_0$ structure, detected by X-ray diffraction (XRD). When the ribbon was manually grinded to powder the phase fraction of 14M phase almost disappeared. Therefore, this typical process to obtain randomly oriented samples for experiments, such as X-ray diffraction, may jeopardize the actual properties and microstructure of the original sample and must be taken into account to consider reported analyses from the literature. Finally, it is also found that martensitic transition in melt-spun $Ni_{55}Fe_{19}Ga_{26}$ is very sensitive to thermal treatments. The transformation shifts to lower temperatures as the samples become previously heated up to higher temperatures (in the range 473 to 623 K, below the temperature of formation of the γ phase) [23].

A large number of applications are developed from these types of materials based on their solid-state martensitic transformations (MT). In the case of Ni-Fe-Ga alloys, MT temperature can be tuned through controlling its composition [8,24]. In general, it has been found that increasing Fe content at a fixed Ga content, the MT temperature decreases [11]. In addition to composition, other parameters, as the heating/cooling rate, can influence the magnetostructural behavior of a material. In fact, it has been found that MT temperature strongly depends on this parameter in different shape memory alloys, as Ti-Ni-Cu [25], Ni-Mn-Sn [26] and Ni-Fe-Ga [27].

In this work we have studied the kinetics of transformation from 14M modulated martensite to austenite phase in a $Ni_{55}Fe_{19}Ga_{26}$ Heusler alloy prepared by melt-spinning on heating at different heating rates. Although a broad distribution in the kinetic parameters is found, it does not prevent performing an average and coherent analysis.

2. Materials and Methods

The alloy with nominal composition $Ni_{55}Fe_{19}Ga_{26}$ was prepared in an induction furnace using high-purity elements (>99.9%). The ingots were melted several times in order to ensure homogeneity. About 30 g of the ingot were melted in a quartz tube under argon atmosphere and ejected onto a rotation wheel with a surface velocity of 25 m/s. Microstructural characterization and stability of $Ni_{55}Fe_{19}Ga_{26}$ melt spun Heusler alloy can be found elsewhere [23].

The martensitic transformation was recorded by differential scanning calorimetry (DSC) using a Perking-Elmer DSC7 (Perkin-Elmer, Norwalk, CT, USA) under Ar flow. Different heating rates (β from 5 to 80 K/min) were used for non-isothermal treatments. Measured temperature was corrected at different heating rates using the melting temperatures of In (429.75 K) and Pb (600.62 K) standards (errors below 0.5 K). The mass of the analyzed pieces of ribbon was around the same of the In standard (10–20 mg).

X-ray diffraction (XRD) patterns were recorded at different temperatures and atmospheres in a Bruker D8C diffractometer (Bruker, Karlsruhe, Germany) using Cu-Kα, λ = 1.5406 Å.

3. Results

Although some previous results corresponding to powder obtained from ribbons are commented above, all the results presented in this work correspond to samples in ribbon shape.

Figure 1a shows in situ XRD patterns of the melt-spun ribbons obtained at the indicated temperatures in ambient atmosphere at the region where is expected to observe the (220) austenite peak. For comparison, Figure 1b shows the XRD patterns obtained in vacuum. In both cases the martensitic transformation from monoclinic 14M modulated martensite phase to cubic $L2_1$ austenite phase can be identified. Even a qualitative comparison of the XRD patterns reveals that martensite phase appears at a much lower temperature when the experiments are performed in vacuum. Two things prevent a quantitative discussion: XRD patterns must be affected due to sample evolution during the acquisition of the data and, in order to minimize this, the acquisition time must be reduced. Moreover, the highly textured polycrystalline character of the ribbons could produce significant differences in the intensities of peaks with respect to the powder standard. Even though, in vacuum conditions the transition is clearly observed at lower temperatures than that found at ambient pressure. The pressure dependence of the martensitic transformation in Heusler alloys has already been reported for other compositions [28,29]. For example, Hamilton et al. [12], observed the influence of external pressure application on martensitic and intermartensic transitions in single crystal of $Ni_{54}Fe_{19}Ga_{27}$. They also found that the higher the applied pressure, the higher the austenite start temperature. Most of the literature found describes that the austenite start temperature shifts to higher temperatures when an extra pressure is applied. This is in line with our present data, although the range of applied pressure is generally increasing the pressure from tens of MPa to GPa, whereas we decrease the pressure down to 10^{-5} mbar. Unlike the previous permanent effects found in the ribbon samples due to high pressure application [23], which produced an intermartensitc transformation from the modulated to the non-modulated $L1_0$ structure, the effects of submitting the sample to vacuum are reversible. Both the modulated 14M phase and transition temperature are recovered once ambient atmosphere is recuperated.

The thermal behavior of $Ni_{55}Fe_{19}Ga_{26}$ ribbons was analyzed by DSC. Samples of the as-melted ribbon preheated at 473 K were submitted to thermal cycles through the martensitic transformation. When each cycle reached the same maximum temperature, 473 K (Figure 2a), the transformation peak temperature decreases after the first heating, but it keeps constant in the subsequent cycles. However, increasing the maximum temperature in successive cycles clearly shifts the transition to lower temperatures, as shown in ref. [23]. All these features, along with the pressure dependence described above, point to a strong influence on the transition of the strain fields present in each sample piece of

ribbon, which are somehow relaxed after heating. On the other hand, the austenite phase obtained in the melt-spun ribbon is expected to have some disordering degree, which should decrease with high temperature treatments. In fact, by heating up the samples to temperatures higher than 600 K, the martensitic transformation temperature as well as the heat of transformation significantly decrease, which is associated with atomic ordering and composition stabilization due to the precipitation of the gamma phase [23]. However, these processes are prevented in our samples as the maximum treatment temperature is 473 K.

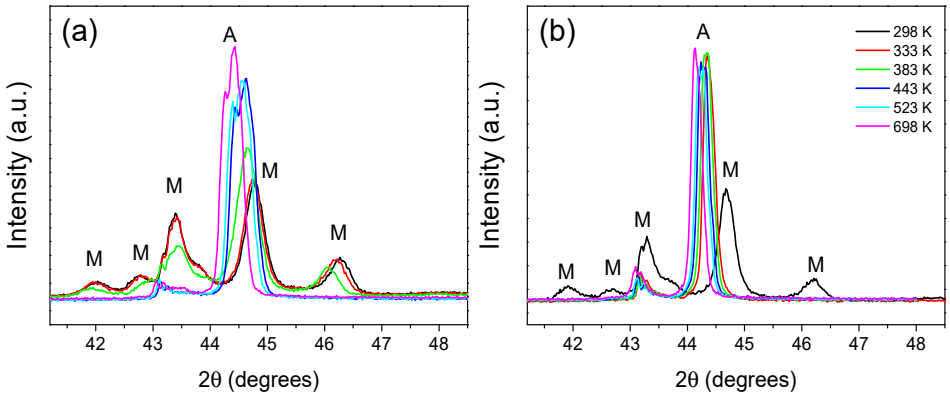

Figure 1. X-ray diffraction (XRD) patterns of as-melt spun $Ni_{55}Fe_{19}Ga_{26}$ obtained at the indicated temperatures at (**a**) ambient atmosphere and (**b**) vacuum (~10^{-5} mbar). "M" and "A" represent the Bragg peaks of the 14M martensite and austenite phases, respectively.

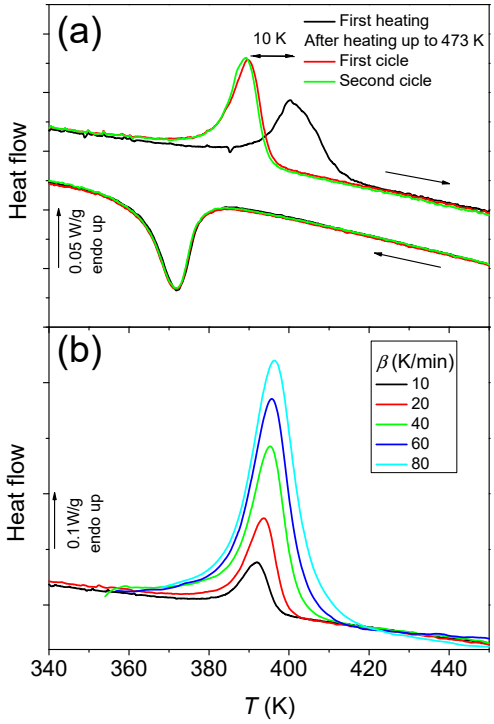

Figure 2. Consecutive differential scanning calorimetry (DSC) scans of a $Ni_{55}Fe_{19}Ga_{26}$ piece of ribbon showing the effect of thermal cycling on the transformation peak temperatures when (**a**) they are heated up to the same maximum temperature and (**b**) they are heated at different heating rates each time.

Figure 2b shows the non-isothermal DSC scans taken at different heating rates for the same piece of ribbon after preheated up to 473 K. A shift of the transition to higher

temperatures can be observed with the increase of β, indicating the thermally activated character of the martensitic transformation.

Figure 3 shows the martensitic transformation registered at 40 K/min for different pieces of the as-melted ribbon. The absence of repetitiveness in the DSC scans of different as-cast ribbon pieces indicates that subtle differences seem to strongly affect the transition, possibly due to local inhomogeneities in composition (below the resolution of fluorescence and energy dispersive spectroscopy measurements done) or to presumably stress fields induced during the production of the ribbon. In order to show the reproducibility of the equipment used, DSC scans of the melting transition of the indium standard are displayed in the inset.

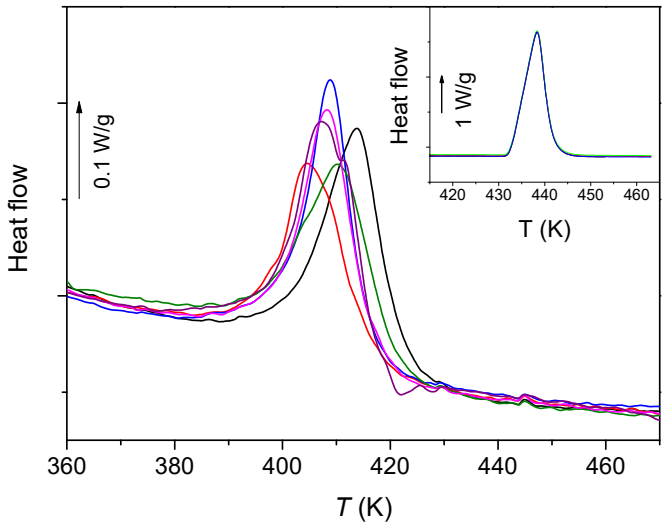

Figure 3. DSC scans of different pieces of as-melt spun ribbon. Inset shows the DSC scans of the In standard.

In order to compile the dispersion of the DSC data, Figure 4 shows the values of the onset, T_{onset}, peak, T_{peak} and end, T_{end}, temperatures. Both T_{onset} and T_{end} were estimated as the intersection between the corresponding maximum slopes with the baseline. The data correspond to the martensitic transformation of as-melt spun ribbon pieces (empty symbols) and ribbon pieces after a previous heating up to 473 K (filled symbols). It can be clearly observed that the dispersion in the characteristic temperatures of the transition is reduced after heating up to 473 K, although the dispersion still exists. On the other hand, a general shift to lower temperatures is observed for samples previously heated up to 473 K (an example is the data on single pieces shown in Figure 2). Moreover, a shift to higher temperatures as the heating rate increases can be observed for T_{peak} (and T_{end}), which indicates the thermally activated character of the martensitic transformation. However, results indicate that heating rate has minor influence on T_{onset}. This is in agreement with the findings of Wang et al. [25]; herein, it has been shown that increase in heating rate results in larger variation of T_{end} than of T_{onset} in Ti-Ni-Cu shape memory alloys, in agreement with their previous work, in which they designed a model of martensitic transformation as a thermally activated process by a chemical and a non-chemical term in the Gibbs free energy [30]. Similar results have also been reported for Ni-Fe-Ga alloys [27].

Figure 5 shows the enthalpy of transformation as a function of the heating rate, which increases with the heating rate from ~3.5 W/g for β = 10 K/min to ~5 W/g for β > 40 K/min. The observed enthalpy tendency has been observed previously [31] and explained by the existence of dislocations associated with high heating rates which generate an internal stress state [32].

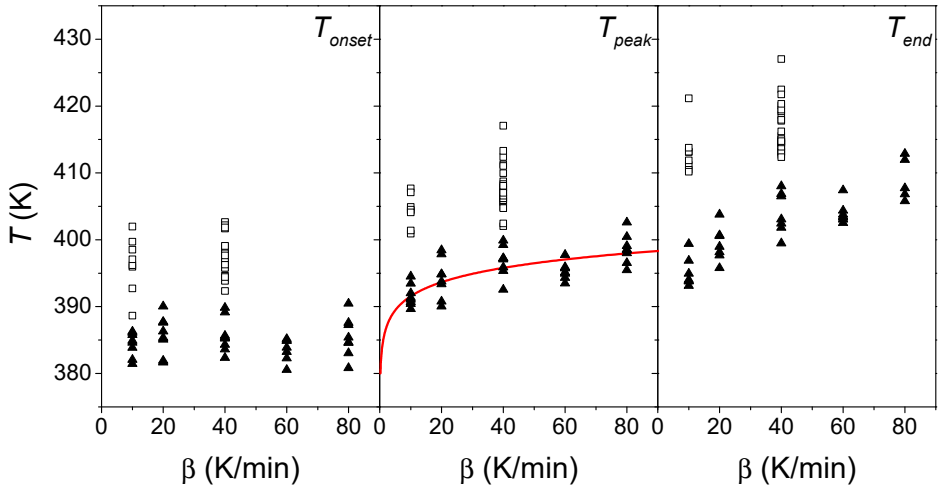

Figure 4. Temperatures corresponding to onset, T_{onset}, peak, T_{peak} and end, T_{end}, of martensite to austenite transformation as a function of the heating rate, β. Empty symbols (about 20 DSC experiments) correspond to as-melt spun ribbon and filled symbols (about 60 DSC experiments) correspond to ribbon pieces after heating up to 473 K. Predicted dependence of T_{peak} from Kissinger's plot is shown as a red line.

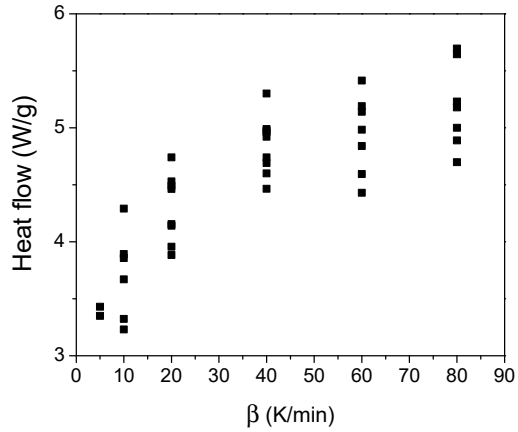

Figure 5. Enthalpy of the martensitic transformation (on heating) as a function of the heating rate for ribbon pieces preheated up to 473 K (about 60 DSC experiments are shown).

4. Discussion

Kissinger method [33] is generally applied to determine the apparent activation energy in thermally activated processes and particularly in the martensitic transformation of Heusler alloys (Ni-Mn-Ga [34], Ni-Mn-Sn [35], Cu-Ni-Al [36]). Figure 6 shows the Kissinger's plots for three pieces of ribbon on which successive DSC scans were performed using β increasing from 10 to 80 K/min. Moreover, other data points corresponding to single DSC scans performed on different sample pieces at different β values are added to the figure. Although results for single samples (squares, circles or triangles) can be relatively well fitted to a straight line (leading to Q_{Kis} values around 500 kJ/mol), the values of the activation energy differ between the different analyzed pieces of ribbon and the cloud of points evidences the dispersion of the data. Moreover, the obtained value is higher than that obtained for $Ni_{55}Fe_{18}Ga_{26}$ prepared by arc-melting, which martensite transformation occurs at around 300 K [27]. These results suggest the importance of the samples fabrication process. This feature can be understood in the frame of the strong effect of subtle differences (i.e., strain fields induced in the ribbon) between the sample pieces. This could be also linked to the probabilistic character of the avalanches phenomenon recently used to describe martensitic transitions [13].

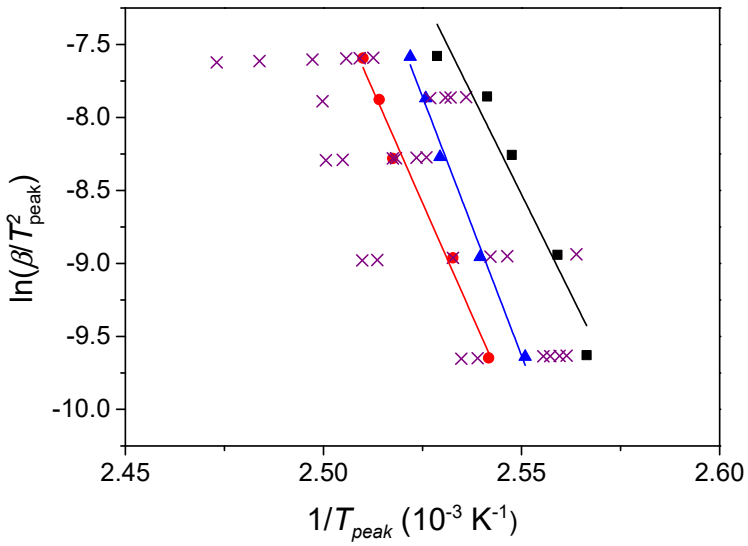

Figure 6. Kissinger's plots for the peak temperature of the martensitic transformation. Filled symbols correspond to data obtained for three pieces of ribbon on which successive DSC scans were performed using β increasing from 10 to 80 K/min. Crosses correspond to data obtained from single DSC scans performed on different sample pieces at different β.

Although the utility of Kissinger's method can be considered in terms of comparative results with those reported in the literature, we cannot neglect that the high dispersion in the parameters of the transition may yield deviations from Kissinger's requirements (e.g., constant transformed fraction at T_{peak} is not fulfilled). As commented in the introduction section, the martensitic transformation can be described as a first order auto-catalytic transformation. From Equation (3), the change in X between two different times or temperatures can be obtained as (thus, avoiding the inherent undefined point at $X = 0$):

$$\int_{X_0}^{X} \frac{dX}{X(1-X)} = \int_{T(X_0)}^{T} \frac{k_M}{\beta} dT \rightarrow -ln\left(\frac{1}{X} - 1\right) + ln\left(\frac{1}{X_0} - 1\right) = \int_{T(X_0)}^{T} \frac{k_M}{\beta} dT, \quad (4)$$

which, if the temperature dependence of k_M can be neglected, leads to:

$$X(t) = \frac{X_0}{(1 - X_0)e^{-\frac{k_M}{\beta}(T - T_0)} + X_0}, \quad (5)$$

where $T_0 = T(X_0)$.

On the other hand, the value of k_M can be obtained from expression (3) as:

$$k_M(T) = \frac{dX}{dt} \frac{1}{X(1-X)}, \quad (6)$$

where $X(T) = \int_0^T \frac{dX}{dt} \beta dT$ and $\frac{dX}{dt} = \frac{1}{\Delta H} \frac{dH}{dt}$ are obtained normalizing the experimental data of heat flow recorded in the DSC. Generally, an Arrhenius dependence is proposed for the frequency factor, characterized by an activation energy, Q, with $k_M(T) = k_{M0} exp\left(-\frac{Q}{RT}\right)$. In order to evaluate this dependence, Figure 7 shows $ln(k_M)$ vs. $1/T$ in the $0.10 < X < 0.99$ range for different β values corresponding to a single sample submitted to scans at different heating rates. A complete figure with the different samples studied in this work is supplied as supplementary material (Figure S1).

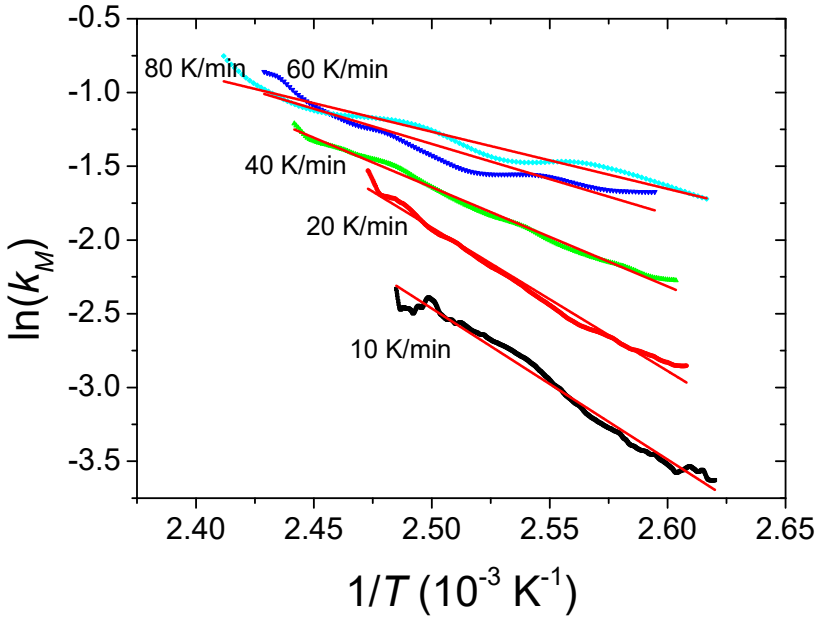

Figure 7. Expected linearity from Arrhenius behavior of the frequency factor $k_M(T)$ for different heating rates (results for a single piece of sample are shown).

Linearity is observed for each curve of Figure 7 (or Figure S1) but the parameters (slope and intersect) depend on β, as it is shown in Figure 8 for the three sample pieces studied at successive β along with results from DSC scans on samples heated at a single β. This figure also shows a common almost linear decrease of Q (and of $ln(k_{M0})$) with β but dispersion of the data is found. A decrease of Q with β has been also reported for other Heusler alloys (Ni-Mn-In-Mg [19] or Ni-Mn-Sn ribbons [35]). This decrease can be understood considering that the observable mechanism of transformation is nucleation (due to the very fast growth). Classical nucleation theories show that the nucleation rate is [14]:

$$I(T) = Ae^{-\frac{\Delta G_c}{RT}}, \tag{7}$$

where ΔG_c is the difference in molar Gibbs energy between the nuclei of the product phase with a critical radius and the starting phase. This magnitude is inversely proportional to the square of the overheating, ΔT^2. As β increases, the transition from martensite to austenite shifts to higher temperatures and, thus, ΔT increases, leading to a decrease in ΔG_c. When only nucleation phenomena is recorded (due to the fast growth in martensitic transformations), ΔG_c can be identified with Q. Therefore, this trend in the activation energy should be generally found in this type of transformations. In the supplementary material, Figure S2 shows a roughly linear trend between $Q^{-0.5}$ and T_{peak}, using the average values obtained in this study. However, the Q values obtained from Kissinger's method are about five times larger than the average value deduced from $k_M(T)$ and, thus, the comparison with literature might be done with caution. On the other hand, there is a clear interdependence between the frequency prefactor k_{M0} and the activation energy Q, which implies a compensation effect [37,38]. The relationship between $ln(k_{M0})$ and Q is evidenced in Figure 9 as a straight line:

$$ln(k_{M0}) = ln(k_{00}) + mQ, \tag{8}$$

with $ln(k_{00}) = -0.5 \pm 0.3$ (k_{00} in Hz) and $m = (2.81 \pm 0.05)10^{-4}$ mol/J. The reliability of the fitting line and the original data were evaluated based on the correlation coefficient, being r^2 = 0.9990. This result can be used to redefine the Arrhenius dependence of k_M to:

$$k_M(T) = k_{00}e^{-\frac{Q(1-mRT)}{RT}}, \tag{9}$$

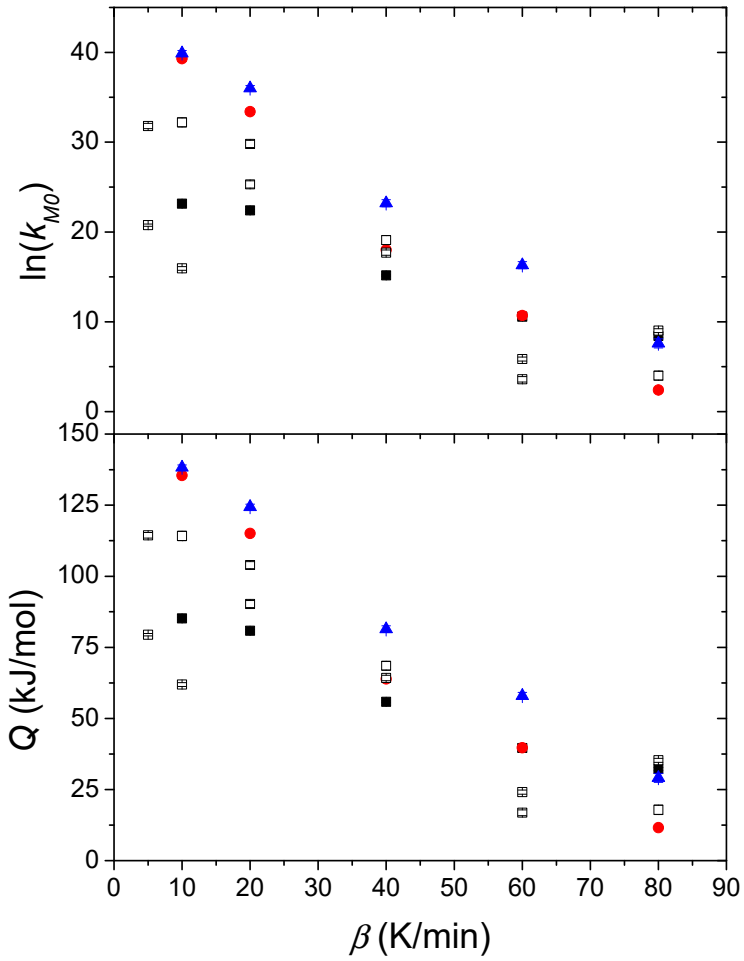

Figure 8. Heating rate dependence of the frequency prefactor, k_{M0} and the activation energy, Q, describing the Arrhenius equation of $k_M(T)$. Solid symbols correspond to experiments performed in a single sample at different heating rates. Hollow symbols correspond to individual measurements in different samples.

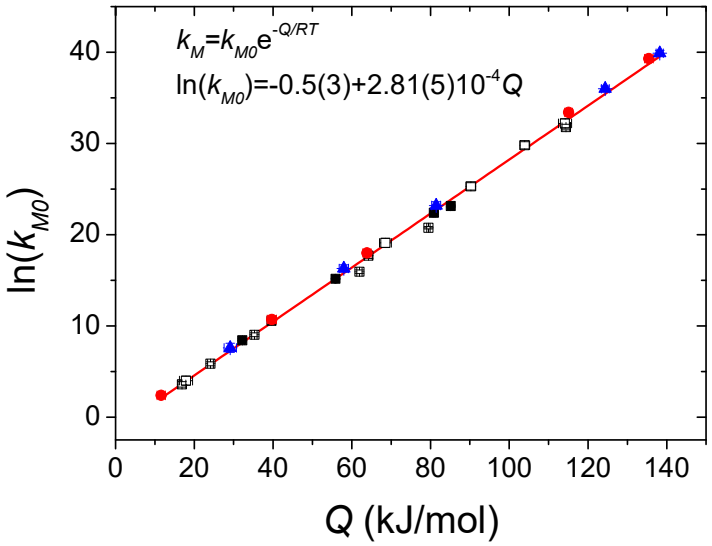

Figure 9. Compensation effect evidenced by a linear correlation between $ln(k_{M0})$ and Q. Different solid symbols correspond to three samples measured at different heating rates. Hollow symbols correspond to individual experiments. The equation for the linear regression (red line) is also shown.

This yields a much lower average value of $Q(1 - mRT)$ for the transition temperature range than those from Kissinger's method (one order of magnitude) and predicts an athermal transformation for $T_{ath} = \frac{1}{mR} = 428 \pm 8\ K$, which is coherently above the measured end temperatures (see black triangles in Figure 4, right panel). In this sense, it has been recently proposed that there is not a clear distinction between athermal and isothermal martensitic transformations, with some experimental results indicating an isothermal character for transformations that were previously considered athermal (Cu-based [39], Ti-Ni based [40] or Ni-Mn-Ga [41] shape memory alloys). Moreover, it has been reported that the transformation of Ni-Fe-Mn alloys changes from isothermal to athermal under the influence of a magnetic field, while the transformation of binary Fe-Ni alloys changes to isothermal under the application of hydrostatic pressure [42]. In fact, Planes et al. [39] showed that isothermal and athermal nature of the martensitic transformation is not intrinsic; the nature of the transformation is directly related to the experimental conditions, which is in agreement with the model of Kakeshita et al. [43].

Taking into account the temperature dependence of $k_M(T)$, Equation (4) must be rewritten:

$$-ln\left(\frac{1}{X} - 1\right) + ln\left(\frac{1}{X_0} - 1\right) = \int_{T(X_0)}^{T} \frac{k_M}{\beta} dT = \int_{T(X_0)}^{T} \frac{k_{00}}{\beta} e^{mQ} e^{-\frac{Q}{RT}} dT, \tag{10}$$

and a more general new equation must substitute for Equation (5):

$$X(t) = \frac{X_0}{(1 - X_0)e^{-B(T)} + X_0}, \tag{11}$$

with $B(T) = \int_{T(X_0)}^{T} \frac{k_{00}}{\beta} e^{mQ} e^{-\frac{Q}{RT}} dT$ only depends on Q. Although this integral could be solved numerically, a simplified form could be proposed assuming a linear Taylor expansion around T_0. Thus, an analytical, but approximate, solution is obtained for the transformed fraction:

$$X = \frac{X_0}{(1 - X_0) \cdot exp\left\{ \frac{k_{00}}{\beta} e^{Q\left(m - \frac{1}{RT_0}\right)} \cdot \left(1 + \frac{Q}{RT_0^2} \frac{(T - T_0)^2}{2}\right) \right\} + X_0}, \tag{12}$$

Once the values of k_{00} and m have been determined (see Figure 9), Q values can be obtained by matching the transformed fraction of just one temperature (e.g., the peak temperature) and the complete curve of $X(T)$ can be built. Figure 10 shows two examples of experimental curves (at β = 10 and 80 K/min respectively) along with the corresponding theoretical curves predicted from Equation (12) in the range $0.1 < X < 0.99$. In these plots, T_0 corresponds to the temperature at which $X_0 = 0.269$ (i.e., $ln\left(\frac{1}{X_0} - 1\right) = 1$) and Q has been determined impossing the value of X at T_{peak}. The values of Q obtained are in agreement with those expected from Figure 8. It is worth mentioning that, despite the evident dispersion of the transition data (as shown in Figure 4), a general equation can satisfactorily describe the kinetics of martensitic transition in the studied melt-spun alloy. This equation is determined by only the transformed fraction at two different temperatures.

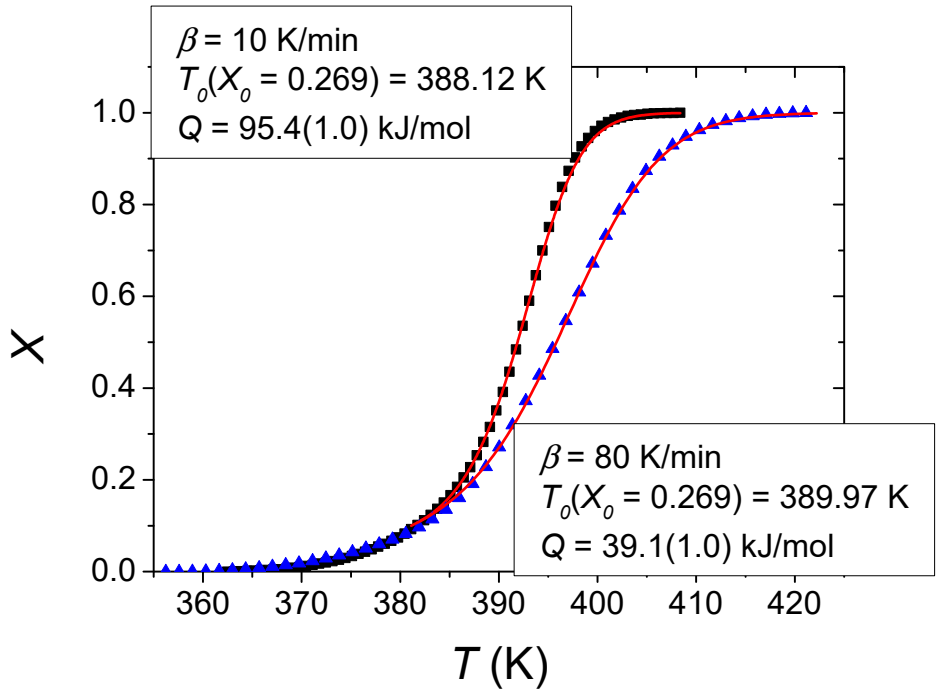

Figure 10. Experimental data (symbols) and theoretical results (lines) of austenite fraction as a function of the temperature for two different DSC heating experiments at 10 and 80 K/min. Corresponding parameters used in Equation (12) are shown in the boxes.

5. Conclusions

Kinetics behavior in the reverse martensitic phase transformation from modulated 14M martensite phase to austenite phase in melt spun $Ni_{55}Fe_{19}Ga_{26}$ ribbons has been analyzed. The heterogeneity of melt spun ribbons affects the martensitic transformation and leads to a strong dispersion of the parameters that characterize it. However, this dispersion can be attenuated after heat treatments at low temperatures leading to a relaxation of the stored stresses.

The high growth rate of the phases involved in martensitic transitions prevents the direct application of the JMAK theory to their kinetic study, characterized by values of the Avrami exponent lower than unity during the whole transformation due to the loss of information of the growth process. In order to overcome this limitation, it has been proposed to describe the martensitic transformation as a first-order autocatalytic process, in which the transformation rate is proportional to the phase fractions of the initial and final products. This description allows to us to satisfactorily describe the transformation, which successfully reproduces the experimental data and is clearly dependent on the heating rate: enthalpy of transformation increases and activation energy decreases as heating rate increases. The latter result is in agreement with the determinant character of the nucleation process (and the not observable effect of the growth mechanism), the driving force of which enhances as the separation from the equilibrium temperature increases. Moreover, the dependence of the activation energy on the heating rate predicts a temperature at which the process would be athermal, which could reveal the nature of martensitic transformation occurring in different family of Heusler materials. Finally, the compensation effect found between activation energy and the frequency factor implies a non-negligible entropic contribution in the activation of the transformation.

Supplementary Materials: The following are available online at https://www.mdpi.com/article/10.3390/met11060849/s1.

Author Contributions: Conceptualization, A.F.M.-G., R.L.-M., J.S.B.; methodology, A.F.M.-G., R.L.-M., J.J.I., J.S.B.; formal analysis, A.F.M.-G., R.L.-M., J.S.B.; investigation, A.F.M.-G., R.L.-M., J.S.B.; resources, C.F.C., A.C., P.S.S.; writing—original draft preparation, A.F.M.-G., R.L.-M., J.S.B.; writing—review and editing, A.F.M.-G., R.L.-M., J.J.I., J.S.B., C.F.C., A.C., P.S.S. All authors have read and agreed to the published version of the manuscript.

Funding: This work was supported by US/JUNTA/FEDER-UE (Grant No. US-1260179), Consejería de Economía, Conocimiento, Empresas y Universidad de la Junta de Andalucía (Grant No. P18-RT-746), University of Sevilla under VI PPIT-US program. Support of projects VEGA [grant number 2/0144/21] and APVV [grant number APVV-19-0369] is acknowledged. A.F.M.-G. acknowledges his contract to the VPPI-US of the University of Sevilla.

Data Availability Statement: The raw/processed data required to reproduce these findings cannot be shared at this time as the data also forms part of an ongoing study.

Conflicts of Interest: The authors declare no conflict of interest.

References

1. Ullakko, K.; Huang, J.K.; Kantner, C.L.S.; O'Handley, R.C.; Kokorin, V.V. Large magnetic-field-induced strains in Ni2MnGa single crystals. *Appl. Phys. Lett.* **1996**, *69*, 1966–1968. [CrossRef]
2. Gràcia-Condal, A.; Gottschall, T.; Pfeuffer, L.; Gutfleisch, O.; Planes, A.; Mañosa, L. Multicaloric effects in metamagnetic Heusler Ni-Mn-In under uniaxial stress and magnetic field. *Appl. Phys. Rev.* **2020**, *7*, 41406. [CrossRef]
3. Krenke, T.; Acet, M.; Wassermann, E.F.; Moya, X.; Mañosa, L.; Planes, A. Ferromagnetism in the austenitic and martensitic states ofNi−Mn−Inalloys. *Phys. Rev. B* **2006**, *73*, 174413. [CrossRef]
4. Yu, S.Y.; Liu, Z.H.; Liu, G.D.; Chen, J.L.; Cao, Z.X.; Wu, G.H.; Zhang, B.; Zhang, X.X. Large magnetoresistance in single-crystalline Ni50Mn50−xInx alloys (x = 14–16) upon martensitic transformation. *Appl. Phys. Lett.* **2006**, *89*, 162503. [CrossRef]
5. Graf, T.; Felser, C.; Parkin, S. Simple rules for the understanding of Heusler compounds. *Prog. Solid State Chem.* **2011**, *39*, 1–50. [CrossRef]
6. Pons, J.; Cesari, E.; Segui, C.; Masdeu, F.; Santamarta, R. Ferromagnetic shape memory alloys: Alternatives to Ni–Mn–Ga. *Mater. Sci. Eng. A* **2008**, *481–482*, 57–65. [CrossRef]
7. Álvarez-Alonso, P.; Aguilar-Ortiz, C.; Villa, E.; Nespoli, A.; Flores-Zúñiga, H.; Chernenko, V. Conventional and inverse elastocaloric effect in Ni-Fe-Ga and Ni-Mn-Sn ribbons. *Scr. Mater.* **2017**, *128*, 36–40. [CrossRef]
8. Pal, D.; Mandal, K. Magnetocaloric effect and magnetoresistance of Ni–Fe–Ga alloys. *J. Phys. D Appl. Phys.* **2010**, *43*, 455002. [CrossRef]
9. Morito, H.; Fujita, A.; Oikawa, K.; Ishida, K.; Fukamichi, K.; Kainuma, R. Stress-assisted magnetic-field-induced strain in Ni–Fe–Ga–Co ferromagnetic shape memory alloys. *Appl. Phys. Lett.* **2007**, *90*, 62505. [CrossRef]
10. Zhang, H.-R.; Wu, G.-H. Atomic-size effect on the microstructural properties of Ni2FeGa. *Acta Mater.* **2011**, *59*, 1249–1258. [CrossRef]
11. Barandiarán, J.M.; Chernenko, V.A.; Lázpita, P.; Gutiérrez, J.; Feuchtwanger, J. Effect of martensitic transformation and magnetic field on transport properties of Ni-Mn-Ga and Ni-Fe-Ga Heusler alloys. *Phys. Rev. B* **2009**, *80*, 104404. [CrossRef]
12. Hamilton, R.; Sehitoglu, H.; Efstathiou, C.; Maier, H. Inter-martensitic transitions in Ni–Fe–Ga single crystals. *Acta Mater.* **2007**, *55*, 4867–4876. [CrossRef]
13. Pérez-Reche, F.-J.; Stipcich, M.; Vives, E.; Mañosa, L.; Planes, A.; Morin, M. Kinetics of martensitic transitions in Cu-Al-Mn under thermal cycling: Analysis at multiple length scales. *Phys. Rev. B* **2004**, *69*, 64101. [CrossRef]
14. Christian, J. *The Theory of Transformations in Metals and Alloys*; Pergamon Elsevier Science: Oxford, UK, 2002.
15. Johnson, W.A.; Mehl, R.F. Reaction kinetics in processes of nucleation and growth. *Am. Inst. Min. Met. Eng.* **1939**, *135*, 416.
16. Avrami, M. Kinetics of Phase Change. I General Theory. *J. Chem. Phys.* **1939**, *7*, 1103–1112. [CrossRef]
17. Avrami, M. Kinetics of Phase Change. II Transformation-Time Relations for Random Distribution of Nuclei. *J. Chem. Phys.* **1940**, *8*, 212–224. [CrossRef]
18. Kolmogorov, A.N. A statistical theory for the recrystallisation of metals. *Bull. Acad. Sci. USSR Phys. Ser.* **1937**, *1*, 355.
19. Zhou, Z.; Yang, L.; Li, R.; Li, J.; Hu, Q. Martensitic transformations and kinetics in Ni-Mn-In-Mg shape memory alloys. *Intermetallics* **2018**, *92*, 49–54. [CrossRef]
20. Blazquez, J.S.; Millán, M.; Conde, C.F.; Conde, A.; Amiano, C.F.C. Nanocrystallization kinetics under instantaneous growth approximation: Experiments and cellular automata simulations. *Phys. Status Solidi* **2010**, *207*, 1148–1153. [CrossRef]
21. Koistinen, D.; Marburger, R. A general equation prescribing the extent of the austenite-martensite transformation in pure iron-carbon alloys and plain carbon steels. *Acta Met.* **1959**, *7*, 59–60. [CrossRef]
22. Burke, J. *The Kinetics of Phase Transformations in Metals*; Pergamon: Oxford, UK, 1965.
23. Manchón-Gordón, A.; Ipus, J.; Kowalczyk, M.; Wójcik, A.; Blázquez, J.; Conde, C.; Maziarz, W.; Švec, P.; Kulik, T.; Conde, A. Effect of pressure on the phase stability and magnetostructural transitions in nickel-rich NiFeGa ribbons. *J. Alloys Compd.* **2020**, *844*, 156092. [CrossRef]

24. Recarte, V.; Pérez-Landazábal, J.; Gomez-Polo, C.; Sánchez-Alarcos, V.; Cesari, E.; Pons, J. Vibrational and magnetic contributions to the entropy change associated with the martensitic transformation of Ni–Fe–Ga ferromagnetic shape memory alloys. *J. Phys. Condens. Matter* **2010**, *22*, 416001. [CrossRef] [PubMed]
25. Wang, Z.; Zu, X.; Huo, Y. Effect of heating/cooling rate on the transformation temperatures in TiNiCu shape memory alloys. *Thermochim. Acta* **2005**, *436*, 153–155. [CrossRef]
26. Kalbfleisch, A.-S.; Matthews, G.; Jacques, P.J. On the influence of the cooling rate on the martensitic transformation of Ni–Mn–Sn Heusler alloys. *Scr. Mater.* **2016**, *114*, 121–124. [CrossRef]
27. Yu, H.; Zu, X.; Fu, H.; Zhang, X.; Wang, Z. Effect of annealing and heating/cooling rate on the transformation temperatures of NiFeGa alloy. *J. Alloys Compd.* **2009**, *470*, 237–240. [CrossRef]
28. Zhang, Y.; Li, Z.; Xu, K.; Kang, Y.; Cao, Y.; Qin, N.; He, X.; Wei, S.; Zeng, H.; Jing, C. Effect of hydrostatic pressure on martensitic transformation and low-temperature magnetic properties in Ni45Cu5Mn35In15 Heusler alloy. *J. Magn. Magn. Mater.* **2021**, *528*, 167835. [CrossRef]
29. Xiao, H.; Wang, R.; Xu, L.; Yang, F.; Yang, C. Pressure effect of magnetic and electronic properties of Mn 2 PtGa Heusler alloy. *Phys. Lett. A* **2018**, *382*, 224–230. [CrossRef]
30. Huo, Y.; Zu, X.; Li, A.; Wang, Z.; Wang, L. Modeling and simulation of irradiation effects on martensitic transformations in shape memory alloys. *Acta Mater.* **2004**, *52*, 2683–2690. [CrossRef]
31. Ben Fraj, B.; Zghal, S.; Tourki, Z. DSC Investigation on Entropy and Enthalpy Changes in Ni-Rich NiTi Shape Memory Alloy at Various Cooling/Heating Rates. In *Proceedings of the 2nd Annual International Conference on Material, Machines and Methods for Sustainable Development (MMMS2020)*; Springer Science and Business Media LLC: Cham, Switzerland, 2018; pp. 631–639.
32. Nurveren, K.; Akdogan, A.; Huang, W. Evolution of transformation characteristics with heating/cooling rate in NiTi shape memory alloys. *J. Mater. Process. Technol.* **2008**, *196*, 129–134. [CrossRef]
33. Kissinger, H.E. Reaction Kinetics in Differential Thermal Analysis. *Anal. Chem.* **1957**, *29*, 1702–1706. [CrossRef]
34. Sánchez-Alarcos, V.; Pérez-Landazabal, J.; Gomez-Polo, C.; Recarte, V. Influence of the atomic order on the magnetic characteristics of a Ni–Mn–Ga ferromagnetic shape memory alloy. *J. Magn. Magn. Mater.* **2008**, *320*, e160–e163. [CrossRef]
35. Zheng, H.; Wu, D.; Xue, S.; Frenzel, J.; Eggeler, G.; Zhai, Q. Martensitic transformation in rapidly solidified Heusler Ni49Mn39Sn12 ribbons. *Acta Mater.* **2011**, *59*, 5692–5699. [CrossRef]
36. Recarte, V.; Pérez-Landazábal, J.; Ibarra, A.; Nó, M.; Juan, J.S. High temperature β phase decomposition process in a Cu–Al–Ni shape memory alloy. *Mater. Sci. Eng. A* **2004**, *378*, 238–242. [CrossRef]
37. Brown, M.E.; Galwey, A.K. The significance of "compensation effects" appearing in data published in "computational aspects of kinetic analysis": ICTAC project, 2000. *Thermochim. Acta* **2002**, *387*, 173–183. [CrossRef]
38. Mianowski, A.; Radko, T.; Siudyga, T. Kinetic compensation effect of isoconversional methods. *React. Kinet. Mech. Catal.* **2021**, *132*, 37–58. [CrossRef]
39. Planes, A.; Pérez-Reche, F.-J.; Vives, E.; Mañosa, L. Kinetics of martensitic transitions in shape-memory alloys. *Scr. Mater.* **2004**, *50*, 181–186. [CrossRef]
40. Kustov, S.; Salas, D.; Cesari, E.; Santamarta, R.; Van Humbeeck, J. Isothermal and athermal martensitic transformations in Ni–Ti shape memory alloys. *Acta Mater.* **2012**, *60*, 2578–2592. [CrossRef]
41. Hürrich, C.; Roth, S.; Pötschke, M.; Rellinghaus, B.; Schultz, L. Isothermal martensitic transformation in polycrystalline Ni50Mn29Ga21. *J. Alloys Compd.* **2010**, *494*, 40–43. [CrossRef]
42. Kakeshita, T.; Saburi, T.; Shimizu, K. Effects of hydrostatic pressure and magnetic field on martensitic transformations. *Mater. Sci. Eng. A* **1999**, *273–275*, 21–39. [CrossRef]
43. Kakeshita, T.; Kuroiwa, K.; Shimizu, K.; Ikeda, T.; Yamagishi, A.; Date, M. A New Model Explainable for Both the Athermal and Isothermal Natures of Martensitic Transformations in Fe–Ni–Mn Alloys. *Mater. Trans. JIM* **1993**, *34*, 423–428. [CrossRef]